Determination of optical constants in noble gases through multiphoton ionization measurements

Wanda R. Ferrell,* M. G. Payne, and W. R. Garrett
Chemical Physics Section, Oak Ridge National Laboratory, Oak Ridge, Tennessee 37831
(Received 7 October 1986)

A multiphoton ionization technique involving third-harmonic generation in phase-matched mixtures of noble gases has been used to make accurate determinations of oscillator strengths for transitions from the ground state to $6s$, $6s'$, $5d$, and $7s$ levels in Xe and to the $5s'$ level of Kr. The method also allows determinations to be made of the absorption coefficients for third-harmonic photons generated in noble-gas mixtures and the vacuum-uv refractive index for the positively dispersive buffer-gas component of the medium, all in the same experiment. The effects of low concentrations of dimers on refractive indexes are also demonstrated. Results are compared with data from other experimental techniques.

I. INTRODUCTION

Atomic oscillator strengths of resonant transitions and vacuum-ultraviolet indexes of refraction and absorption coefficients of gaseous media are important in such areas as atomic theory, plasma physics, astrophysics, and nonlinear optics. Unfortunately, experimental values of these parameters are not accurately known in many spectral regions. Since most experimental techniques[1–8] for measuring these quantities are based upon use of an optical spectrometer, difficulties are encountered in their determination in the special region below 100 nm. This wavelength restriction is due in large part to the transmission properties of available windows.

Reported methods which have been utilized in the determination of oscillator strengths, and which are not limited by windows, are high-energy electron spectroscopy,[9] atomic beam methods,[10] and optical phase-matching techniques.[11–15] The present method falls in the last category.

In phase-matching techniques, properties of nonlinear optical mixing are used to determine an oscillator strength, or F value, for the transition with which the nonlinear process is associated. Puell and Vidal[11] first demonstrated that relative oscillator strengths could be determined through measurements of phase-matched sum frequency generation with unfocused laser beams. Later Wynne and Beigang[12] used the method of Puell and Vidal, improved through the use of tunable dye lasers, to measure F values in Ca. Mahon and Thompkins[13] also used the method for measurements in Hg, with the added improvement of iterating a series of relative F values to obtain improved accuracy.

In a different phase-matching method involving focused beams and the use of a buffer gas, Kramer *et al.*[15] determined a vuv oscillator strength in Xe. With a focused geometry, results can be complicated by the complex mode structure of the laser beam, where the effects on harmonic production are predictable but tedious.[16] This complication was avoided in Ref. 15 by working at high pressure where results became independent of mode structure. Also, in cases where a buffer gas has been used, its refractive index at the wavelength in question must be available independently.

Finally, in a very recent study Smith and Alford[4] have presented two new methods for measuring oscillator strengths, based on sum frequency generation. Their methods require two unfocused laser beams in one method and three in the other to obtain an F value for the transition associated with the generated light.

In previous work by the present investigators, detailed theoretical[17–20] and experimental studies[21–23] have been made of multiphoton ionization (MPI) processes that occur in negatively dispersive media where third-harmonic fields can strongly influence MPI observations. In the latest of these studies[23] a new plane-wave phase-matching technique was developed for the determination, in one experiment, of vuv oscillator strengths, the refractive index at 3ω of buffer gases used to produce phase matching, and the absorption coefficient for the third-harmonic light in generation media consisting of an active gas and a high concentration of buffer gas. We note that in nonlinear frequency generation schemes information on the absorption coefficient and linear indices is needed and often not available in vuv wavelength regions. (Castex,[24] e.g., has measured absorption coefficients in noble-gas mixtures with a double spectrometer scheme, which was also wavelength limited by window transparency.)

For comparative purposes we note that the method developed in Refs. 20 and 23, and more fully utilized here, is similar in style and phase-matching content to the work of Puell and Vidal. However, important differences in, and extensions of, their method give the present technique additional merit. First, by using a high concentration of buffer gas, phase matching is achieved at a relatively small detuning from exact resonance. Thus, the optical properties of the active gas are totally dominated by the resonant transition under consideration and an absolute F value is obtained. Moreover, by measuring the number densities, the phase-matching position and the third-harmonic profile widths, the linear index of the buffer gas and the absorption coefficient of the medium can also be determined. Indeed, the absorption-induced "distortion" of the third-harmonic profile mentioned by Puel and Vi-

dal[11] (and avoided in all previous experiments) is quantitatively described and used to determine the absorption coefficient. Finally, by measuring ionization yields rather than photon output, the present method can be extended to vuv regions where direct photon measurements would be complicated by window opacities.

II. OPTICAL PARAMETERS FROM MULTIPHOTON IONIZATION MEASUREMENTS

In the earlier study mentioned above,[20] a very detailed theoretical description was given of multiphoton ionization processes in phase-matched noble-gas mixtures in regions near three-photon resonances. The theoretical study provided the method used here to determine oscillator strengths, refractive indexes, and absorption coefficients. We will not repeat the analysis, but we will recall the features of multiphoton ionization measurements under phase-matched unfocused third-harmonic generation which are relevant to the present application and summarize the analytical results which provide the basis of analysis used here.

We consider third-harmonic generation, and the concomitant multiphoton ionization processes, in the negatively dispersive region of three-photon resonances of an active gas A with a positively dispersive buffer gas B that is present to produce phase matching. With unfocused laser beams, third-harmonic production occurs only in a narrow frequency region around that which produces $\Delta k = k_{3\omega} - 3k_{\omega} = 0$, where Δk is the difference between the third-harmonic wave vector $k_{3\omega}$ and fundamental wave vectors $3k_{\omega}$, within the nonlinear medium. In our treatment the total phase mismatch is conveniently subdivided into three terms. The first is a real nonresonant contribution, Δk_R, which is essentially constant over the negatively dispersive frequency region of interest and which is contributed almost entirely by the buffer gas B (since the buffer-gas number density N_B must be much larger than the active gas number density N_A, in order to phase match). Also, we define a resonant contribution due to the strong dipole coupling at 3ω between the ground state $|0\rangle$ and the excited state $|1\rangle$ of the active species. This term is strongly frequency dependent and is proportional to the product of N_A and the absolute square of the dipole matrix element D_{01} (or oscillator strength F_{01}) between $|0\rangle$ and $|1\rangle$. It has the form $\Delta k_{\rm res} = -2\pi N_A \omega_r |D_{01}|^2/(\hbar c \Delta_r)$, where $\hbar\omega_r$ is the energy of the resonant state $|1\rangle$ and Δ_r is the detuning of the third-harmonic frequency from ω_r (i.e., $\Delta_r = +3\omega - \omega_r$). In the actual procedure Δ_r is chosen to be small enough to assure that $\Delta k_{\rm res}$ totally dominates the contribution from the active gas. Finally, there is an imaginary nonresonant component $-i\beta$ which is due to absorption of the third-harmonic photons by the medium. The phase mismatch is thus expressed[19] as $\Delta k = -\Delta k_R + \kappa/\Delta_r - i\beta$, where

$$\kappa = 2\pi N_A \omega_r |D_{01}|^2/\hbar c = \pi N_A (e^2/mc) F_{01} ,$$

and 2β is the absorption coefficient for the generated third-harmonic light. The frequency at which phase matching occurs (peak value of third-harmonic production) is that for which the real part of Δk vanishes—or at $\Delta k_R + \kappa/\Delta_r = 0$. The detuning, Δ_r, at which this condition is satisfied is defined as $\Delta_r \equiv \Delta_m = -\kappa/\Delta k_R$. In terms of the linear susceptibility χ_B or index of refraction $n_B(\omega)$ the detuning from resonance for phase matching can be written in the form

$$\Delta_m = \frac{e^2 F_{01}}{(6m\omega/c)[\chi_B(\omega) - \chi_B(3\omega)]} \frac{N_A}{N_B} = \frac{2\pi e^2 F_{01} N_A}{n_B(\omega) - n_B(3\omega)} . \quad (1a)$$

The displacement from resonance of exact phase matching can be rewritten in terms of the wavelength shift $\Delta\lambda_m$, rather than frequency shift Δ_m:[25,26]

$$\Delta\lambda_m = \lambda_r - \lambda_m = C P_A / P_B , \quad (1b)$$

where λ_r is the wavelength of the three-photon resonance and λ_m is the (laser) wavelength at which $\Delta k = 0$.

The phase-matching frequency can be varied over the negatively dispersive region of a given transition by adjusting the ratio of P_A to P_B and the phase-matching factor C of Eq. (1b) can be determined experimentally (the value of C is not strictly constant, but is a slowly varying function of λ).

In order to predict experimentally observed behavior of third-harmonic production and MPI processes, we choose a chaotic field model for the laser and a Gaussian line shape of the form

$$I(\omega) = (2\pi\sigma^2)^{-1} \bar{I} \exp[-(\omega - \bar{\omega})^2/2\sigma^2] . \quad (2)$$

Here the laser has central frequency $\bar{\omega}$, with bandwidth σ and mean intensity $\bar{I}$. Statistical averages over fluctuations in the laser produce frequency dependencies and absolute amplitudes for MPI signals which can be compared with experiment, as was done in the study by Garrett *et al.*[23] In the latter study, all experimental findings were in close agreement with the theoretical predictions of Ref. 20.

For an unfocused laser with bandwidth σ [or frequency distribution of Eq. (2)] the predicted flux of third-harmonic photons at depth z in a nonlinear absorptive medium was derived analytically as

$$F_{3\omega}(z,t) = 4N_A \left[\frac{\Delta_m}{\sigma}\right]^2 \frac{|\bar{\Omega}_3(t - z/c)|^2}{\Gamma_1 \kappa} \times \int_0^{\xi} d\eta\, e^{-\eta^2} \cos(\delta_1 \eta)(e^{-\Gamma_1 \eta} - e^{-(2\xi - \eta)\Gamma_1}) . \quad (3)$$

In this expression $\bar{\Omega}_3(t)$ is the three-photon Rabi frequency at the mean power density

$$\bar{\Omega}_3(t) = \alpha(\omega)(\langle E_0^2(t)\rangle)^{3/2} ,$$

where $E_0(t)$ is the laser pulse amplitude and

$$\alpha(\omega) = \sum_n \sum_m D_{0,n} D_{n,m} D_{m,1} [(2\hbar)^3 (\omega_n - \omega_0 - \omega) \times (\omega_m - \omega_0 - 2\omega)] .$$

The laser pulse envelope's length in time is large as compared to $1/\sigma$. The evaluation of the third-harmonic flux,

as a function of displacement δ from exact phase matching ($\delta=\Delta_r-\Delta_m$), was reduced to an integration involving reduced variables $\delta_1=\sqrt{2/3}\delta/\sigma$; $\Gamma_1=\sqrt{2/3}(\gamma_{01}/2+\Delta_m^2\beta/\kappa)/\sigma$ and $\xi=\sqrt{3/2}\sigma\kappa z/\Delta_m^2$, where δ_1 is a reduced detuning from the position of exact phase matching; Γ_1 is a reduced effective width for the profile of third-harmonic output and ξ is a reduced z coordinate along the unfocused laser beam.[20] Note that Γ_1 includes an explicit width contribution due to absorption at 3ω.

As described previously,[20,23] the ionization rate in a phase-matched noble-gas mixture arises almost entirely from partial absorption of the third-harmonic flux (with absorption coefficient 2β). For a laser with a Gaussian spatial beam profile of radius d, where d is large enough for diffraction effects to be negligible, the total rate of atomic excitation within an active volume of length L extending between z_1 and z_1+L is given by the volume integral of the product of third-harmonic flux and the absorption coefficient

$$R_{\rm exc}(\delta,t)=2\beta\int_{z_1}^{z_1+L}dz\int_0^\infty d\rho\,2\pi\rho e^{-6\rho^2/d^2}F_{3\omega}(z,t)$$
$$=\frac{4\pi\sqrt{2}N_A\beta d^2}{3\sqrt{3}}\left[\frac{\Delta_m^4}{\sigma^3}\right]\frac{|\bar{\Omega}_3(t)|^2}{\Gamma_1\kappa^2}$$
$$\times[G_0(\xi_2,\Gamma_1,\delta_1)-G_0(\xi_1,\Gamma_1,\delta_1)]\ . \tag{4}$$

The function $G_0(\xi,\Gamma_1,\delta 1)$, which results from the integration of $F_{3\omega}$ over the volume of the laser beam, is given by

$$G_0(\xi,\Gamma_1,\delta_1)=\int_0^\xi dn\,e^{-n^2}\cos(\delta_1 n)\left[(\xi-n)e^{-\Gamma_1 n}-\frac{1}{2\Gamma_1}(e^{-\Gamma_1 n}-e^{-\Gamma_1(2\xi-n)})\right]\ . \tag{5}$$

In Eq. (4), $\xi_1=\sqrt{3/2}\sigma\kappa z_1/\Delta_m^2$ and $\xi_2=\sqrt{3/2}\sigma\kappa(z_1+L)/\Delta_m^2$. We assume that the ionization cross section out of the upper state is essentially frequency independent over the limited wavelength range under present consideration, thus the total rate of ion production is proportional to the product of the excitation rate of Eq. (4) and the ionization rate γ_I out of the excited state.[5] The total rate of ion production is thus $R_I=\gamma_I R_{\rm exc}$ where γ_I is assumed frequency independent. However, it is the frequency profile, not the absolute ion yield, which is useful in the present context. The spectral "widths" of the frequency profiles of third-harmonic related ionization signals are dependent on the number density of the buffer gas, the magnitude of displacement from resonance Δ_m, and on the absorption coefficient for the third-harmonic photons.

Through a series of measurements of the widths of third-harmonic profiles, at measured pressures P_A (at fixed P_A/P_B), all at a measured displacement Δ_m, one can obtain the oscillator strength F_{01} of the resonance with which the third-harmonic generation is associated, the absorption coefficient 2β for the generated third-harmonic light in the active-gas–buffer-gas combination, and the linear refractive index of the buffer gas at 3ω. To see the basis for extraction of these quantities from multiphoton ionization measurements we need only look at two limiting cases of the general expression for the ion yield as a function of detuning δ from exact phase matching. That is, we examine the frequency profile ("line shape") for ionization associated with third-harmonic production when phase matching occurs at position Δ_m from three-photon resonance.

First, consider phase-matched third-harmonic generation in a region of length L at low concentration where the absorption of the generated photons per unit distance in the nonlinear medium is small ($\beta L\ll 1$, and ξ_1 and $\xi_2\ll 1$). In this limit the ionization profile about Δ_m reduces to

$$R_I(\delta,t)=\gamma_I 8\pi N_A\beta d^2\frac{\Delta_m^4}{\sigma^2}\frac{|\bar{\Omega}_3(t)|^2}{\kappa^2\delta}\left[\frac{\kappa\delta}{\Delta_m^2}(z_2-z_1)-[\sin(\kappa z_2\delta/\Delta_m^2)-\sin(\kappa z_1\delta/\Delta_m^2)]\right]\ . \tag{6}$$

The third-harmonic induced ionization profile has a full width at half maximum, $\delta_{\rm FWHM}$, which is

$$\delta_{\rm FWHM}\approx 7.3\Delta_m^2/\kappa L=\frac{7.3\Delta_m^2}{L\pi(e^2/mc)N_A F_{01}}\ . \tag{7}$$

References 20 and 23 contain detailed discussions of the third-harmonic ionization signals as number density N_A of the active gas is varied with fixed ratio of active gas to buffer gas density (i.e., fixed N_A/N_B). We simply note here that measurements of $\delta_{\rm FWHM}$, absolute number density N_A, and the detuning from three-photon resonance at which optimum phase matching occurs, Δ_m, yields a value of the oscillator strength F_{01} from Eq. (7). (L is the length of the ionization region over which electrons are collected and measured.) Note also from the above definitions that the phase-matching position Δ_m from Eq. (1a) involves F_{01} and the difference in the refractive indexes of the buffer gas at ω and at 3ω. Thus having determined F_{01} as indicated above, one can determine $n_B(\omega)-n_B(3\omega)$ for the buffer gas by measuring Δ_m, N_A and N_B at an arbitrary position (or pressure ratio). However, the index at the laser frequency $n_B(\omega)$ is accurately known; thus, $n_B(3\omega)$ can be determined from Eq. (1a).

Finally, at high number density, absorption of the third-harmonic photon flux becomes significant, and $\beta L\gg 1$. In this limit $\delta_{\rm FWHM}$ becomes proportional to the absorption coefficient, and the third-harmonic ionization frequency profile becomes Lorentzian[20,23] and can be quite broad. This new analytic result yields

$$R_I(\delta_1 t)=2\pi\gamma_I N_A\beta d^2\frac{\Delta_m^2}{\sigma^2}\frac{|\bar{\Omega}_3(t)|^2}{\kappa}\frac{z_2-z_1}{\delta^2+\Delta_m^4\beta^2/\kappa^2} \tag{8}$$

and

$$\delta_{\mathrm{FWHM}}=2\Delta_m^2\beta/\kappa \ . \tag{9}$$

Thus in the high-pressure regime a measure of δ_{FWHM} and Δ_m completely determines β since previous measurements determined F_{01}, and from Eq. (9),

$$\beta=\pi N_A(e^2/mc)F_{01}\delta_{\mathrm{FWHM}}/2\Delta_m^2 \ . \tag{10}$$

Note that we have used the limiting cases to illustrate how multiphoton ionization measurements at low and high number densities may be used to obtain the three quantities of interest here. In the present study, the theoretical analysis of Ref. 20 provides a quantitative description of the multiphoton ionization process over the negatively dispersive regions of several levels in Xe and Kr in wide spectral and pressure ranges. The data are in close agreement with experiment at all pressures and under all phase-matching frequencies. From the very general theoretical relationship for position, line shape, and pressure dependence of the phase-matched third-harmonic profile, and the corresponding MPI frequency profile (Figs. 4—6), we can extract accurate values for F_{01}, β, and $n_B(3\omega)$ by adjusting values of these constants in a computer-generated match to experimental data at a particular phase-matching frequency. In this way we determine all three parameters simultaneously from one set of experimental data. Of course the data go smoothly into the simple limiting cases described earlier, where the extraction of the optical constants is particularly simple. Note that the analysis can be carried out for any particular ratio of P_A/P_B; that is, at any choice of phase-matching frequency as long as Δ_m is small enough to cause the resonance under consideration to overshadow other contributions to the index from the active gas. This flexibility is important in certain instances, because preexisting active-gas—buffer-gas dimers, though low in concentration, were found to influence the index at certain dimer absorption frequencies. As will be mentioned below, these regions can easily be avoided.

III. EXPERIMENTAL APPARATUS

The experimental setup for multiphoton ionization measurements is shown in Fig. 1. The apparatus consists of a Lumonics Excimer pumped dye laser system, two ionization cells separated by a lithium-flouride window, and an LSI-11/03 computer with related electronics.

A Xe-Cl fill in the Lumonics 861T Series Excimer laser produces an average energy per pulse at 10 Hz of 80 mJ with a pulse length of 4 ns. The absolute energy of the excimer and the dye laser outputs is measured by Scientech model 36-0001 and model 38-0105 energy meters, respectively. These meters are then used to calibrate photodiodes, which monitor the laser intensity for each laser shot. The EDP 330 dye laser operates with typical bandwidth of 0.005 nm.

The ionization chamber is constructed with antireflection-coated entrance and exit windows. It contains a proportional counter which consists of a small-diameter, field-producing collector wire in a counting gas. In the present context the counting gas is the noble-gas mixture under investigation. The dynamics of the counter are such that electrons produced in the gas are accelerated by the radial electric field of the wire, which is held at a constant positive voltage. In the high field regions near the collector wire the initial electrons produce more electrons to give amplification while retaining signals that are proportional to the number of initial electrons. This amplification is a function only of the gas fill and the field strength. Thus, when calibrated, the proportional counter is a very suitable device for the detection of a small number of charges. The counter is calibrated by an internal ^{55}Fe x-ray source.[23] (The ^{55}Fe x rays create 268 electrons when the energy is fully absorbed within the counter volume.) The counter is designed with guard electrodes at either end of the cell to eliminate electrons originating at the entrance and exit windows. This arrangement defines the counting region, which starts and ends 2.3 cm from the entrance and exit windows, respectively, and is 15.0 cm in length. These guard electrodes, in addition to timing discrimination of the electronics, restrict the counting region to the laser ionization volume through which the laser beam passes.

Various mixtures of xenon with either argon or krypton as buffer gases were introduced into this cell for the studies involving phase-matched third-harmonic generation. The absolute partial pressures of the mixtures were deter-

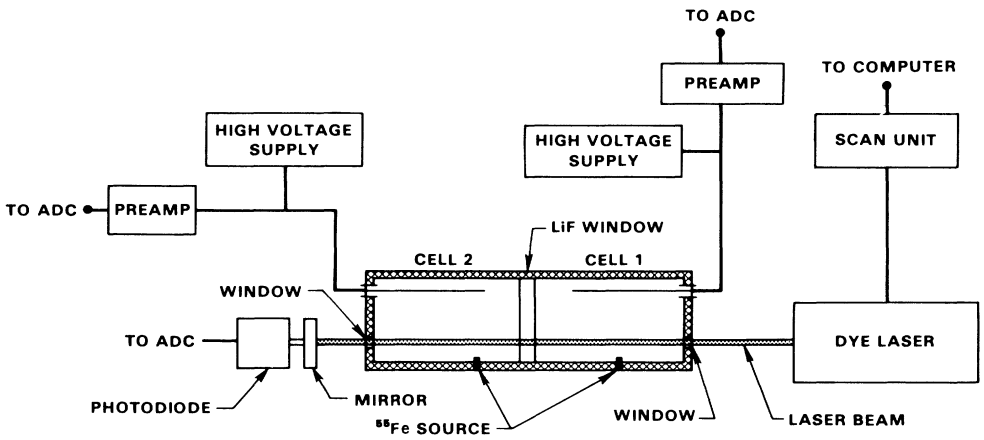

FIG. 1. Experimental apparatus. Laser is Lumonics 861T excimer pump with EDP 330 dye laser.

mined by two capacitance manometers. (MKS Baratrons: one with a head for 0—10-Torr range and the second with an overlapping range of 0—1000 Torr.)

Cell 1 was the primary ionization chamber and contained the experimental gas mixtures. Since the gas mixtures are such that the pressure can be several hundred torr, pressure broadening and the corresponding shifts in three-photon $\Delta J=1$ resonance lines occur. With the laser system available here, accurate determinations of spectral positions could then only be made if the position of a given resonance was unambiguously measured in a low concentration gas fill in cell 2.

IV. EXPERIMENTAL PROCEDURE

The general unfocused beam technique, which has been described earlier and outlined above, was used to determine the oscillator strengths for the $6s(3/2)J=1$, $6s'(1/2)J=1$, and $5d(3/2)J=1$ states of xenon, and the refractive indexes and absorption coefficients of gas mixtures in the regions near these transitions. Mildly focused beams, on the other hand, had to be used in the studies for the $7s(3/2)J=1$ level of xenon and the $5s'(1/2)J=1$ level of krypton, since the available power densities were not sufficient to probe these levels with an unfocused geometry. This limited the results for these levels to oscillator strength determinations only, in contrast to the other levels where the unfocused geometry provided all three quantities.

An arbitrary amount of xenon is first added to the evacuated chamber, and a chosen quantity of a buffer gas is then added to produce a desired ratio P_A/P_B. Sufficient time is then allowed for the gas mixture to equilibrate. The design is such that the mixture becomes uniformly mixed within one or two minutes. The laser is then scanned over the high-energy side of the resonance under investigation. A typical ionization signal record is shown in Fig. 2. Since exact matching occurs at $\Delta k=\Delta k_R+\kappa/\Delta_m=0$, the detuning from resonance of the peak of the observed ionization signal due to phase-matched third-harmonic generation defines the ratio $\kappa/\Delta k_R$. If more buffer gas is added, phase matching occurs at a smaller detuning from the subject resonance. Thus, by increasing the buffer-gas partial pressure at fixed active-gas partial pressure, phase-matching signal can be moved along the high-energy wing of the resonance line under study.[23] By this procedure the region is then "calibrated," i.e., the $C(\lambda)$ for Eq. (1b) is determined.

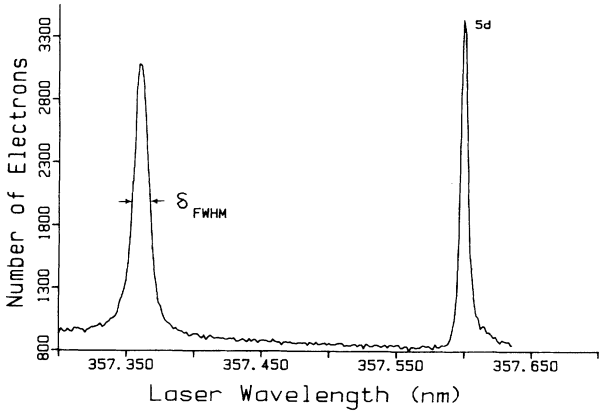

FIG. 2. Wavelength scan of ionization signals resulting from phased-matched third-harmonic production in the negatively dispersive region of the Xe $5d$ level. Resonant signal for three-photon excitation of the $5d$ state on the right. $\Delta k=0$ occurs at detuning $\Delta_m=-0.249$ nm ($P_{Xe}=5.387$ Torr, $P_{Ar}=990.5$ Torr), $\delta_{FWHM}=0.135$ nm.

Once calibration of the phase-matching region for a given resonance is completed, the active and buffer gases can be introduced to the chamber in various proportions to the chamber to achieve phase-matched third-harmonic production at any given vuv frequency within the negatively dispersive region of a resonance. The dependency of the absorption of 3ω is then eliminated by keeping the ratio of the gases and thus the position of the phase-matched signal constant. The determination of the optical parameters is made from the dependence of the width of the ionization signals on the partial pressure of the resonant species at a fixed phase-matched frequency, determined by the constant ratio P_A/P_B. If the gases are thoroughly mixed and if differential pumping has been eliminated, the partial pressure of xenon can be effectively varied by a corresponding change in the total pressure. Data are acquired at constant phase-matching frequency, by successively pumping a given gas mixture to lower total pressure.

Since the position and widths of the phase-matching signal are the basis of this analysis, accurate measurements of these two parameters are essential to accurate determinations of the desired optical parameters. The widths of the ionization profiles are determined by a least-squares-fitting routine. These measured widths are then plotted as a function of xenon partial pressure. The resulting curve of pressure-dependent widths is subsequently fit by an iterative process in which β and Δk_R are varied for the best fit.

Figures 3—5 demonstrate the effective fitting of the phase-matching curves (third-harmonic intensity profile) to the theoretical shapes at different Xe pressures with Ar buffer gas. All three scans were made for a fixed ratio of component gases ($P_{Xe}/P_{Ar}=0.018$). In Fig. 3 the Xe partial pressure is 12.01 Torr, and the fit to the Lorenztian, or high pressure shape, is compared with the fit to the low-pressure shape given by Eq. (6). For this particular data where $\Gamma_1 \gg \xi$ and $\beta L \gg 1$, the Lorentzian (high-pressure limit) line shape of Eq. (8) is seen to be the better choice. A similar comparison is given in Fig. 4 for a phase-matching curve which is generated at a lower total pressure of 325.2 Torr or $P_{Xe}=5.75$ Torr. The better fit for this curve is the expression given by Eq. (6). The conditions for this curve, then, are such that the absorption effects are negligible and the generation volume is determined by the physical limits of the chamber. The theory predicts for these conditions that signal amplitudes are quartic in xenon pressure, and the widths should be inversely proportional to xenon pressure. Finally, the expected behavior at even lower pressure is shown in Fig. 5. The signal is shown to both decrease in amplitude and broaden dramatically as the xenon partial pressure is re-

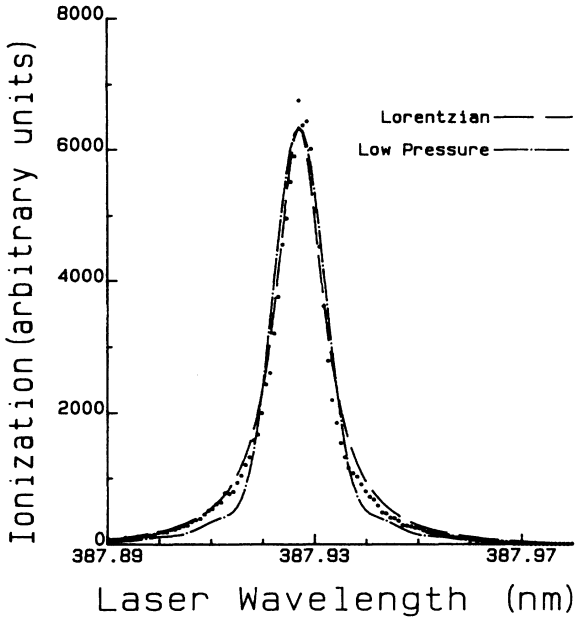

FIG. 3. Contrast of the Lorentzian and low-pressure fits to a phase-matched ionization signal. Dashed line represents Lorentzian curve, which is the better fit for these data. Xenon partial pressure is 12.01 Torr.

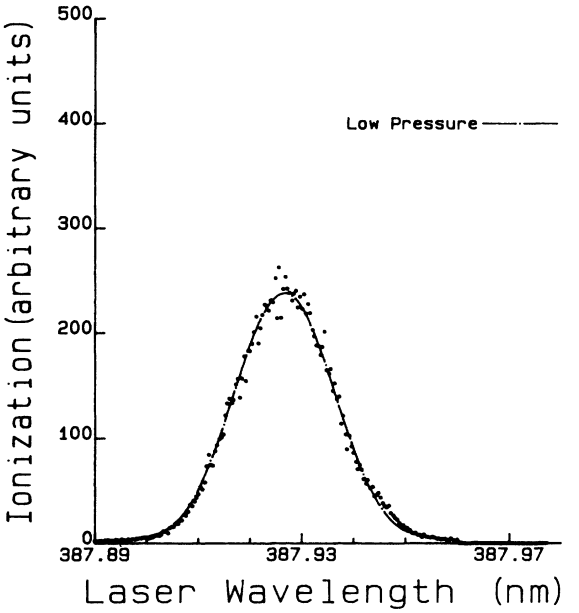

FIG. 5. Subsequent broadening of the phase-matched third-harmonic profile occurs as xenon pressure is reduced to 2.99 Torr, in close agreement with theoretical prediction of shape and width.

duced from 5.75 to 2.99 Torr. The signals in Figs. 3 and 5 were recorded with attenuated laser intensity to effect accurate measurements—that is, to avoid space-charge problems in the counter and saturation effects in the preamplifier. The resulting signals in these figures have been normalized to the intensity and gain of Fig. 4 in order to accurately illustrate the pressure-amplitude relationship. (The phase-matching position and curve widths are independent of intensity.)

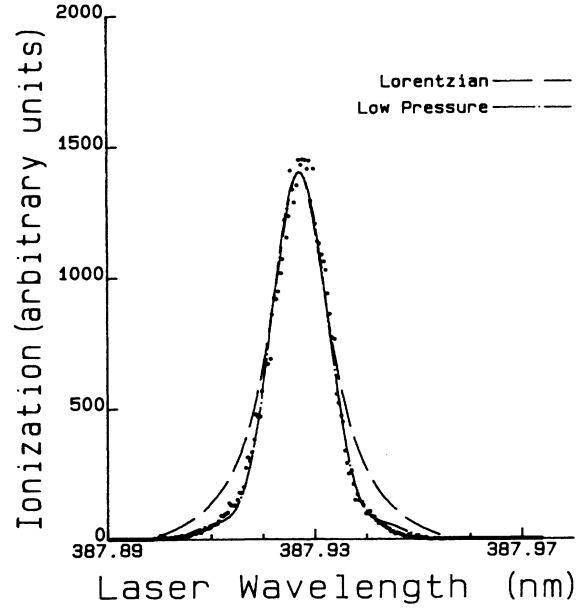

FIG. 4. Contrast of the two computer-generated fits to a phase-matching curve, which displays the low-pressure shape. Xenon partial pressure is 5.75 Torr.

V. EXPERIMENTAL RESULTS

Since all data are acquired separately for each atomic state studied, we first discuss the results for F_{01} and the absorption coefficients according to the transition involved. The information on linear indices of refraction for buffer gas is then summarized for the vuv-wavelength region covered in the present study. Finally, we show that preexisting noble-gas dimers can influence phase-matching conditions in certain narrow-frequency regions of interest herein.

A. Xenon $6s(3/2)J=1$

Most of the results associated with the $6s$ state of Xe reported earlier in Ref 23. We will not repeat any of the details here, but simply note that a value of $F_{01}=0.26\pm0.05$ was obtained in a study with Ar buffer gas and the absorption coefficient at $\lambda_{3\omega}=146.4$ nm was found to be $2\beta=1.0\times10^{-4}P_{\mathrm{Xe}}P_{\mathrm{Ar}}$ where the pressure is in torr. We report additional results obtained by phase matching with Kr buffer gas. Data were obtained at phase-matching frequency corresponding to $\Delta\lambda_m=-1.23$ nm. Within experimental error we again obtained $F_{01}=0.26\pm0.05$, with an absorption coefficient of $4.1\times10^{-4}P_{\mathrm{Xe}}P_{\mathrm{Kr}}$. At this wavelength ($\lambda_{3\omega}=146.55$ nm) Castex[24] gives a value for the absorption coefficient which differs from the present determination by only 2%.

It is also useful to compare the oscillator strength obtained from the present technique to previously determined values of F_{01} for transitions from the ground state

to the $6s$ level of Xe. We note that a wide range of values and quoted accuracies exist for this constant. For example, a low-energy electron impact technique[27] yields 0.183 ± 0.073, an electron-energy-loss technique[9] provides 0.260 ± 0.052, a total absorption technique[7] gives 0.26 ± 0.02, and a line shift technique[2] gives 0.27 ± 0.03. The present value for this constant is quite consistent with previous measurements with an estimated accuracy comparable to the best previous values.

B. Xenon $6s'(1/2)J=1$

As was mentioned previously it is convenient in the present experimental procedure to establish the phase-matching relationship, the $C(\lambda)$ of Eq. (1b), over the negatively dispersive region of a given resonance with a particular choice of phase-matching buffer gas. In Fig. 6 we show an example of $C(\lambda)$ as a function of detuning of the phase-matching position from the $6s$ state of Xe with Kr buffer gas. We use the illustration to make two points about the phase-matching relationship. First, it was found that $C(\lambda)$ was a very smooth function of $P_{\mathrm{Xe}}/P_{\mathrm{Kr}}$ for most of the range of study. However, at certain phase-matching positions, the data departed from the expected trend and showed clearly discernable excursions from an essentially straight-line behavior. This anomalous behavior in the buffer-gas phase-matching contribution was found to be associated with the absorption bands of low concentrations of preexisting Xe-Kr dimers (or Xe-Ar dimers in other examples). In Fig. 6 we show wavelength positions of a few Xe-Kr dimer levels. We will discuss their influence on the phase-matching behavior in Sec. III below. Here we simply note that the present experimental optical constant determinations can be conducted at an arbitrarily chosen position within the negatively dispersive region of a resonance; thus, perturbations of phase-matched third-harmonic production in narrow-frequency regions due to dimer resonances can readily be avoided.

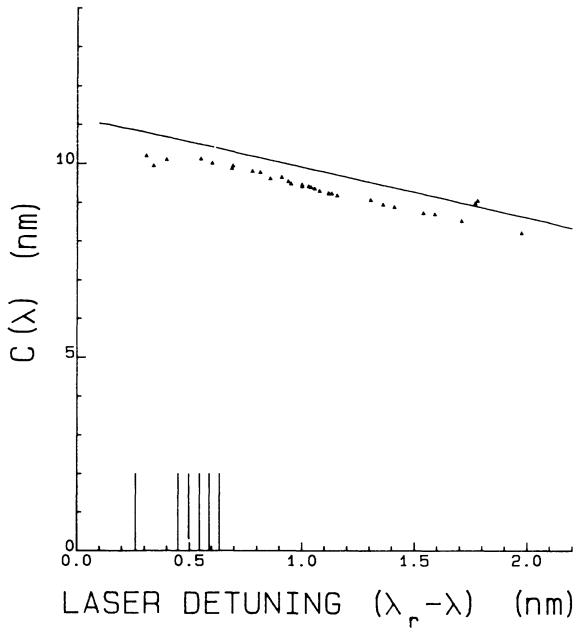

FIG. 6. Phase-matching constant for xenon-krypton mixtures near the $6s'$ level of xenon. Vertical lines represent Xe-Kr dimer absorption bands. The solid curve is the value of $C(\lambda)$ yielded by analysis through a modified Sellmeir formula (see text).

In the course of the analyses of the present study we need an accurate representation of the indexes of refraction for buffer gases in the visible region (where accurate data are available) and in some instances it is useful to be able to correct for a small nonresonant contribution to the index from the active gas. For this purpose of representing the refractive index at any wavelength λ, a Sellmeir formula is used, where generally

$$\eta(\lambda)-1=\frac{Nr_e}{2\pi}\sum_i \frac{F_{i0}}{\lambda_i^{-2}-\lambda^{-2}} ,$$

where $r_e=2.88\times10^{-13}$ cm. Also F_{i0} is the oscillator strength for the ith transition from the ground state at resonance wavelength λ_i (cm). In the actual application of the Sellmeir-type formula for describing $\eta(\lambda)$ only a fraction of the discrete oscillator strengths is known and small continuum contributions are largely unmeasured. We parametrize the equation to include these unmeasured contributions by including two "resonances" which are adjusted to simulate contributions from high-lying bound states and from the continuum to yield close agreement with $\eta(\lambda)$ in the very accurately known region above 200 nm.

Optical parameters associated with the $6s'$ level of Xe were made through MPI measurement in phased-matched Xe-Ar mixtures at a $P_{\mathrm{Xe}}/P_{\mathrm{Ar}}$ ratio of 0.0161. This choice produces a phased-matched third-harmonic production peak at 0.754 nm on the blue side of the $6s'$ level. [At this ratio the value of $C(\lambda)$ is 46.7 nm.] Analysis of the pressure dependent widths of the observed third-harmonic profile (Fig. 7) yields an oscillator strength of 0.190 ± 0.010 and an absorption coefficient at this wavelength $4\times10^{-5}P_{\mathrm{Xe}}P_{\mathrm{Ar}}$. The oscillator strength can be compared to a value of 0.19 by Geiger[9] and 0.169 by Koch.[28]

As a consistency check on the phase-matching analysis it is instructive to compute $C(\lambda)$ for Xe-Kr mixtures for comparison with the data of Fig. 6. The solid line is the theoretical position of $C(\lambda)$ from the known indexes of refraction and the Sellmeir analysis described above.

C. Xenon $5d(3/2)J=1$

The experimental and calculated phase-matching constant for Ar is shown in Fig. 8. The experimental phase-matching constant again bears the signature which attests to the influence of the dimer absorption bands on the index of refraction for nearby regions (see below). An analysis of phase matching at a detuning of -0.248 nm from the $5d(3/2)J=1$ resonance (Fig. 9) yields an oscillator strength of 0.37 ± 0.019. This value compares well with the value 0.395 from earlier studies.[9,24] In addition, this analysis of the data given in Fig. 9 gives the absorption coefficient at 357.361 nm as $6\times10^{-4}P_{\mathrm{Xe}}P_{\mathrm{Ar}}$. In this case, as the xenon pressure is increased, the full width of

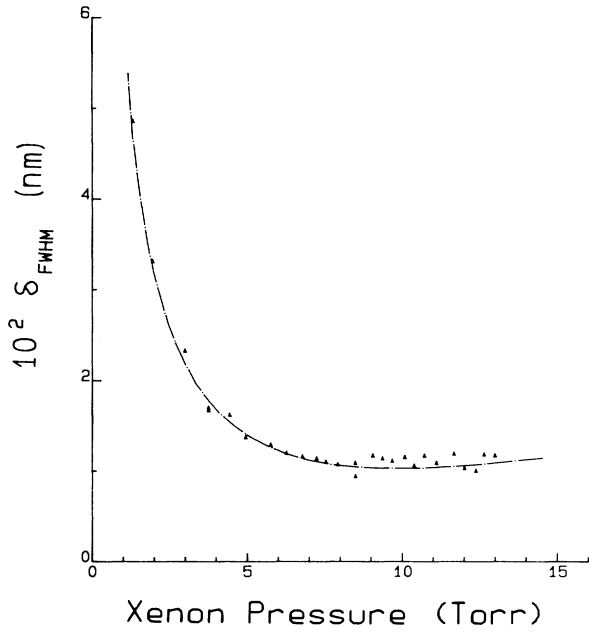

FIG. 7. Pressure relationship of the FWHM of the phase-matching signal near the $6s'$ xenon with argon as a buffer gas. $\Delta\lambda=-0.754$ nm, $F_{01}=0.190$, and $\beta=4\times10^{-5}P_{Xe}P_{Ar}$.

the phase-matching profile goes through a minimum value, 0.043 nm, which is the bandwidth of the laser.[20]

D. Xenon $7s(3/2)J=1$ and krypton $5s'(1/2)J=1$

Wavelengths for three-photon excitation of these two atomic levels lie on the wing of the TMQ dye curve. The

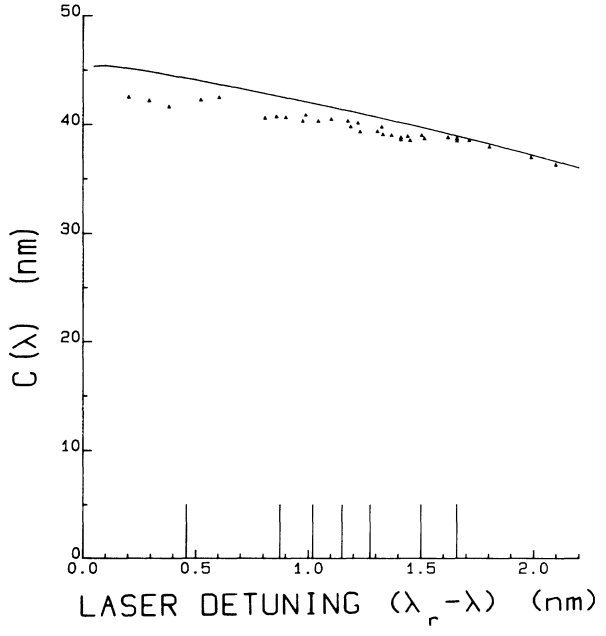

FIG. 8. Phase-matching constant for the $5d$ level of xenon with argon as the buffer gas. Absorption bands for Xe-Ar dimers are shown as vertical lines. Solid line is $C(\lambda)$ from analysis based on a modified Sellmeir equation (see text).

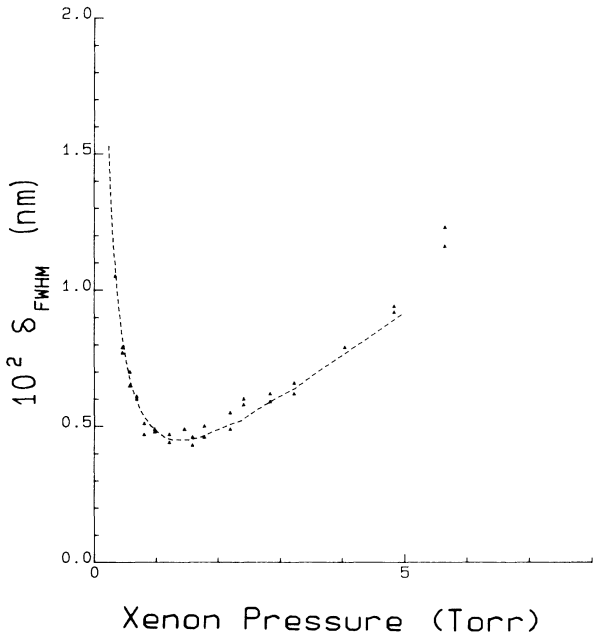

FIG. 9. FWHM of the phased-matched third-harmonic profile as a function of Xe pressure at constant P_{Xe}/P_{Ar} ratio. $\Delta\lambda=-0.248$ nm, from the $5d$ state of Xe, $F_{01}=0.37$, and $\beta=6\times10^{-4}P_{Xe}P_{Ar}$.

low conversion efficiency in this region of the laser dye precluded ionization measurements in an unfocused geometry for these two levels due to low ionization yields. Thus, a focused geometry procedure, which is similar to the technique used by Kramer *et al.*,[15] was utilized in measurements associated with these states. The shapes of the phase-matching curves, in a general medium which includes absorption, can be analyzed in the focused geometry only if the beam profile is accurately known and is Gaussian.

Since the laser system used in the present experiments cannot be so accurately characterized, we cannot simultaneously determine an oscillator strength and the absorption coefficient of the medium in our focused geometry. However, we note that the position of the peaks of phase-matched third-harmonic production is independent of the beam profile. It is determined only by the refractive indexes of the nonlinear medium at ω and 3ω. It has been shown by Kramer *et al.*[15] that with a long-focal-length lens (confocal parameter comparable to the length of the generating medium; $f_l=1$ m in the present instance) and with high number density of the medium, the phase-matching condition is given approximately by $\Delta k_R=0$. If the index of a buffer gas is known, the value of an oscillator strength can be determined by adjusting its value to give the observed position at which phase matching ($\Delta k_R=0$) occurs.[15] But it happens that the $7s$ state in Xe is only 2.16 nm on the low-energy side of the $5d(3/2)J=1$ level which has a much larger oscillator strength. Thus, the expression for Δk must be modified to contain resonant contributions from both $5d$ and $7s$ states. Thus, $\Delta k_R=\kappa_{5d}/\Delta_{5d}+\kappa_{7s}/\Delta_{7s}+\Delta k_{nr}$ where κ_{5d} and κ_{7s} are as defined previously containing the oscillator

strength for the $5d$ and $7s$ states, respectively. Also, Δ_{5d} is the detuning from the $5d$ resonance ($\Delta_{5d}=3\omega-\omega_r$, where $\hbar\omega_r$ is the energy of the $5d$ state) and Δ_{7s} is similarly defined. The term $\Delta k_{\rm nr}$ is the nonresonant contribution to phase mismatch contributed by the buffer gas and that contributed by all other states of Xe.

Now note that F_{01} for the $5d$ state was determined in the previous experiments along the index of the buffer gas in this frequency region. Thus the position at which $\Delta k_R=0$ can be used along with information thus available to determine the value of κ_{7s} (or F_{01} for ground state to $7s$). This procedure yields an oscillator strength of 0.088 ± 0.0088. This value consistently predicts phase-matching points in Xe-Ar mixtures, and that found in pure Xe. We note that on the basis of measurements in Xe-Ar mixtures, the point of phase matching in pure Xe at modest pressures is predicted to be 1.0 nm on the red side of the $7s$ resonance, which is in good agreement with the measured phase-matching point at a laser detuning of 1.428 nm.

In the focused phase-matching technique utilized by Kramer *et al.*, where literature values were utilized for the index of Ar at 3ω, an oscillator strength of 0.0968 ± 0.012 for ground state to $7s$ state was measured. Previous low-angle electron scattering techniques yielded values of 0.11 ± 0.04,[27] 0.0968 ± 0.02,[9] and 0.09 ± 0.02.[26]

A similar focused beam method was used to determine the oscillator strength for the ground state to $5s'$ level of Kr. Utilizing the measured index of Ar at 3ω measurements of the $\Delta k_R=0$ point in Kr-Ar mixtures yields an oscillator strength of 0.18 ± 0.027 for the ground state to $5s'$ state of Kr.

Previously reported values of F_{01} for the ground state to $5s'$ state in Kr are 0.173 by Geiger,[9] 0.135 by Williamson,[6] and 0.266 by Bjorklund.[26] Results on oscillator strengths from the present and previous studies are summarized in Table I.

E. Indexes of refraction

Knowledge of the indexes of refraction for a nonlinear medium in the wavelength region of investigation is critical for assessing the most efficient schemes for generation of higher-harmonic photons. The energy range of the atomic levels in noble gases has made mixtures of these gases ideal nonlinear media for harmonic generation. Therefore, an accurate profile of the vuv indexes for these gases is of special importance in nonlinear frequency generation.

Previously, measurements $\eta(\lambda)$ in the vuv optical range have been accomplished by several different techniques. Some of these are interferometry, spectral line shifts, and Rayleigh scattering. Since most of the previous data in argon and krypton do not coincide with the wavelengths which were experimentally determined in this paper, the validity of the technique is assessed via the Sellmeir formula using a method simiar to that of Mahon *et al.*[29]

Once Δk is known from the above analysis, the vuv index of refraction can be calculated from the expression

$$\Delta k=\frac{3\omega}{c}[n(\omega)-n(3\omega)]\ , \tag{11}$$

where the index of refraction at the fundamental wavelength is determined reliably from available data. From the present study, the three experimental points in argon at STP are $(n-1)/N=2.037\times10^{-23}$ cm^{-3} (119.120 nm), $(n-1)/N=1.637\times10^{-23}$ cm^{-3} (129.309 nm), and $(n-1)/N=1.427\times10^{-23}$ cm^{-3} (146.542 nm). These experimental points vary by only 2% from the calculated indexes (see Fig. 10).

Further evaluation of the present method for vuv index determination can be gotten by comparison of published data with the presently predicted index. Kramer *et al.*[30] in a focused, nonlinear technique measured vuv indexes of refraction in argon, which were in excellent agreement with that predicted by the Sellmeir analysis described above. Chashchina *et al.*[3] measured the indexes of refraction from 230.0–110.0 nm in argon by a spectral line-shift technique. The stated error for these measurements is given as 0.2 to 0.5%. These results are given via a three-term Sellmeir formula with no raw data shown.[31] Chashchina gives $(n-1)/N$ at 140 nm to be 1.487×10^{-23} cm^{-3} which is only 0.1% higher than the present value, at 30 nm $(n-1)/N=1.635\times10^{-23}$ cm^{-3} which is 0.2% lower than present results, at 120 nm $(n-1)/N=1.935\times10^{-23}$ cm^{-3} which is 1% lower than here, and at 118.2 nm $(n-1)/N=2.043\times10^{-23}$ cm^{-3} which is 0.6% lower than the present value.

Since the index of refraction at the Lyman-α wavelength (121.57 nm) is of interest in plasma diagnostics, the index of refraction at this wavelength can be found in the literature. Mahon *et al.*[32] report the calculated value $(n-1)/N=1.92\times10^{-23}$ cm^{-3}, Chashchina *et al.*[3] report 1.87×10^{-23} cm^{-3}, which compares well with the present value of 1.88×10^{-23} cm^{-3}, and Chopra nd Heddle[33] by a Rayleigh scattering technique give 1.90×10^{-23} cm^{-3}. The present formulation only deviates by less than 1% from the two experimental values.

The experimental results from the two krypton studies do not compare as well with the calculated values as in the case for argon. The experimentally determined indexes in krypton are $(n-1)/N=2.607\times10^{-23}$ cm^{-3} at 146.413 nm and $(n-1)/N=2.654\times10^{-23}$ cm^{-3} at 146.550 nm. The respective variations of these two values

TABLE I. Oscillator strengths.

Level	Ref. 9	Ref. 27	Ref. 7	Ref. 2	Ref. 15	Ref. 28	Present study
Xe $6s$	0.26	0.183	0.26	0.27			0.260±0.05
Xe $6s'$	0.19	0.169					0.19±0.04
Xe $5d$	0.395	0.395					0.370±0.07
Xe $7s$	0.0968	0.11			0.098		0.088±0.01
Kr $5s'$	0.173		0.135			0.266	0.180±0.027

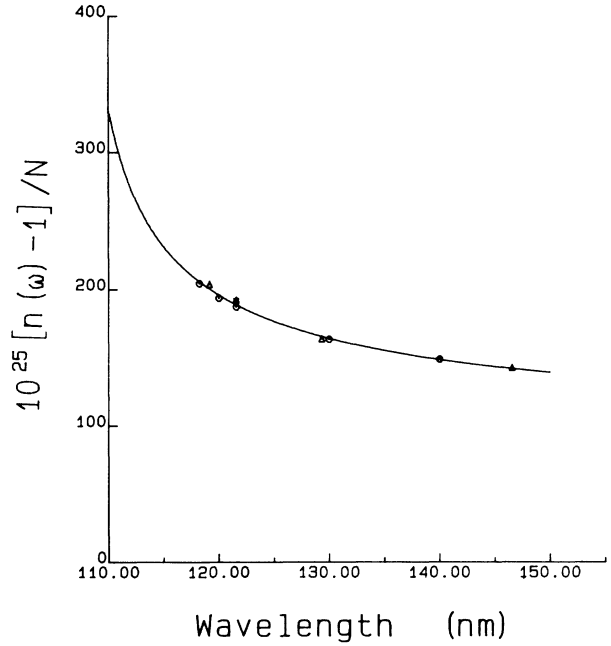

FIG. 10. vuv index of refraction per atom for argon. Solid curve is based on the use of Sellmeir formula incorporating the present results.

from the present Sellmeir calculations are 11% and 2.7%, where both experimental points are higher than the calculated values. The detuning of both of these experimental points is rather large, which may be the source of the greater deviation from the calculated value. One notes that the index of refraction for xenon is approximated by the nearby resonant term in the expression for Δ_m. Of course, as the point of interest moves farther from resonance, this approximation will be less accurate. The buffer-gas contribution to the phase-mismatch expression is also assumed to be constant. In this region, the krypton contribution is relatively flat, but near the 7*s* of xenon, for example, this is not the case. The hypothesis of the source of error being due to the resonant approximation is borne out by the relative errors of the two experimental points.

The index of refraction undergoes very sharp changes in the near-resonance regions, but it is these regions in which phase matching can be attained. Three experimental indexes are reported for 121.6 nm in krypton, which lies to the blue of the first krypton at 123.58 nm Mahon *et al.*[29] report $(n-1)/N=-5.58\times10^{-24}$ cm^{-3} as deduced from the phase matching in pure krypton with a focused beam. Gladushchak *et al.*[4] measured -3.35×10^{-24} cm^{-3} by the phase-matching point in krypton. Since the Rayleigh scattering technique of Chopra and Heddle[33] determines $(n-1)^2$, a positive value was measured, 3.28×10^{-23} cm^{-3} These experimental values are not in very good agreement with each other, and neither do they compare favorably with either Mahon's calculation[27] (-7.75×10^{-24} cm^{-3}) or the present calculation (-4.632×10^{-23} cm^{-3}).

In the more smoothly varying regions for the index, the agreement between present and reported indexes is much better. At 228.8 nm, for example, our analysis gives 1.814×10^{-23} cm^{-3} which agrees to less than 1% with 1.820×10^{-23} cm^{-3} reported by Bideau-Mehu *et al.*,[1] 1.820×10^{-23} cm^{-3} by Smith *et al.*,[5] and 1.828×10^{-23} cm^{-3} by Chashchina *et al.*[3] The index of fraction at 140.1 nm is the closest wavelength to the two experimental points of this study. At this wavelength, results from our analysis vary at most by 2.5%.

The 6*s* region of xenon is the lowest wavelength region for which linear indexes are found in the literature. Bideau-Mehu *et al.*[1] measured 1.895×10^{-23} cm^{-3} for 148.3 nm, which is to the red of the 6*s* level. Chashchina and Shreider[2] found a very similar result, 1.823×10^{-22} cm^{-3}. The 1.829×10^{-22} cm^{-3} as calculated by present analysis varies only 1% from each of these. For a point on the blue side of the 6*s*, the deviations are somewhat larger: 2.433×10^{-23} cm^{-3} by Bideau-Mehu *et al.*,[1] 2.40×10^{-23} cm^{-3} by Chashchina and Shreider,[2] and 2.483×10^{-23} cm^{-3} from present results.

F. Effects of preexisting dimers on phase matching

Our previous analysis of phase-matched third-harmonic production in noble-gas mixtures was based on the approximation of refractive indexes produced by a single "active-gas" resonance with which third-harmonic production is associated and a nonresonant buffer-gas contributor of essentially constant value over the frequency region under investigation. However, as is well known, small concentrations of molecular dimers exist in noble gases at room temperature. Castex[24] reported the ratio of Xe-Kr to free atoms in an equal mixture of 2.69×10^{19} cm^{-3} at 293 K as 0.69%. And, she reported the fraction of Xe-Ar dimers 0.48% at 300 K. In the context of the present experiment Xe-Ar or Xe-Kr dimers will exhibit absorption bands which are shifted a few tens to a few hundreds of wave numbers from a given Xe resonance, mostly on the high-energy side where third-harmonic generation is studied. Even though the dimer concentration is very low, they will interact strongly with third-harmonic light in the frequency region near an absorption band and thereby perturb the absorption coefficient and the linear index at 3ω. Evidence of such perturbations is discernible in the wavelength dependence of the phase-matching function $C(\lambda)$ of Figs. 6 and 8. In the vicinity of Xe-Kr or Xe-Ar dimer bands, respectively, the data depart significantly from an essentially straight-line trend. A dimer contribution to the index, $n(3\omega)$, can be seen in these and other similar data in narrow bands associated with identifiable dimer levels. In Figs. 6 and 8 the positions of the most prominent dimer bands reported by Castex are shown in the figures. One expects a resonant contribution in the phase mismatch from a dimer band where the contribution is proportional to the concentration and inversely proportional to the detuning from the dimer resonance. The contributions are small at 300 K (they could be very significant at reduced temperatures).

The effect of a dimer contribution to Δk can also be seen in the frequency profile for phase-matched third-harmonic production when the frequency region encom-

passes a dimer band. An example of such a phase-matching curve is shown in Fig. 11. The data in this figure are for 20.0 Torr Xe with 899.3 Torr of Kr buffer-gas. Here phase matching ($\Delta k = 0$) occurs at detuning of 0.220 and 0.2270 nm from the $6s'$ level of Xe. Absorption bands exist in this region at 0.270 and 0.450 nm (see Fig. 6). This observation indicates that line shapes for third-harmonic production can be strongly influenced by molecular dimer bands, even at very low concentrations. Note that dimer contributions to Δk relative to that from the atomic resonance and the buffer gas becomes more pronounced at large detunings from the atomic line, and wash out if the dimer band should occur at very small detuning where the wing of the atomic line still produces a large contribution to Δk. In any case, in the context of the phase-matching technique of the present study, one can easily avoid the narrow-frequency regions where dimer perturbations to Δk exist.

VI. CONCLUSION

The present study has shown that in addition to enhancing the harmonic generation process, phase-matching properties can be utilized to make accurate determinations of resonant oscillator strengths of the active gas, absorption coefficients of a mixture of the active gas and a second gas (buffer gas), and the vuv index of refraction for the second gas. This was accomplished through the accurate measurements of the detuning of the exact phase-matching point from three-photon resonance and careful determinations of the widths of the phase-matching curves.

The strength of this phase-matching technique with unfocused laser beams lies not only in the number of parameters which can be measured, but in the absence of wavelength restrictions in the regions of interest. Since no windows are needed for the vuv in the phase-matched ionization measurement technique, the range of examination is limited only by the light source.

In addition, the data suggest the possibility of a detailed investigation of the role of noble-gas dimers in nonlinear frequency generation. The influence of the dimer states on the index, as seen in the phase-matching constants and third-harmonic profiles, seems to indicate the feasibility of such a study.

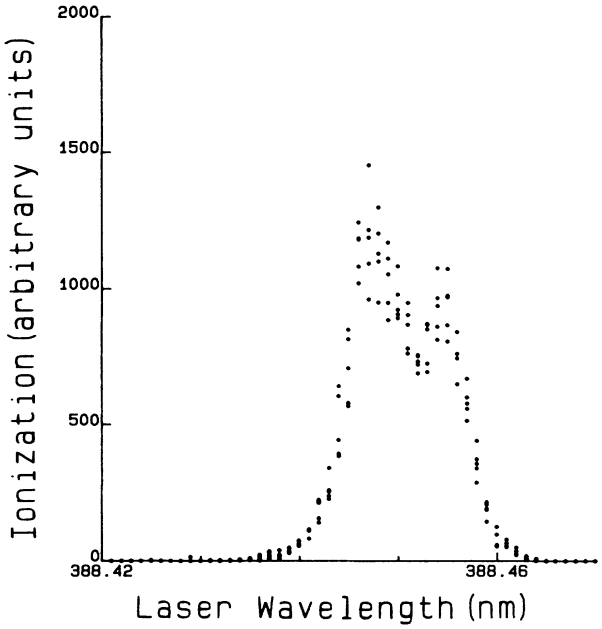

FIG. 11. Phase-matched third-harmonic profile for the $6s'$ level of Xe with Kr buffer gas (20.0 Torr Xe and 899.3 Torr of Kr). For this ratio, P_{Xe}/P_{Kr}, phase matching occurs in the vicinity of a Xe-Kr dimer band. The third-harmonic production profile is strongly perturbed by the dimer contribution to Δk.

Since accurate determinations of detunings of third-harmonic peaks from line center require a measurement of the resonant position which is not perturbed by collision effects, the apparatus is already in place for pressure-broadening studies. These studies have been performed for the four xenon resonances of this investigation, and the results will be published as a separate study.

ACKNOWLEDGMENTS

Research is sponsored by the Office of Health and Environmental Research, U. S. Department of Energy under Contract No. DE-AC05-84OR21400 with Martin Marietta Energy Systems, Inc. W. R. Ferrell was partially supported through Oak Ridge Associated Universities for the U. S. Department of Energy.

*Present address: Department of Energy, Office of Scientific and Technical Information, P.O. Box 62, Oak Ridge, TN 37831.

[1]A. Bideau-Mehu, Y. Guern, R. Abjean, and A. Johannin-Giles, J. Quant. Spectrosc. Radiat. Transfer **25**, 395 (1981).

[2]G. I. Chashchina and E. Y. Shreider, Opt. Spectrosc. **27**, 79 (1969).

[3]G. I. Chashchina, V. I. Gladushk, and E. Y. Shreider, Opt. Spectrosc. **24**, 542 (1968).

[4]V. P. Gladushchak, S. A. Moshkalev, I. Chashchina, and E. Y. Shreider, Opt. Spectrosc. **51**, 608 (1981).

[5]P. L. Smith, W. H. Parnson, and M. C. E. Huber, Opt. Commun. **14**, 374 (1975).

[6]P. G. Wilkinson, J. Quant. Spectrosc. Radiat. Transfer **5**, 503 (1965).

[7]P. G. Wilkinson, J. Quant. Spectrosc. Radiat. Transfer **6**, 832 (1966).

[8]P. G. Wilkinson, J. Quant. Spectrosc. Radiat. Transfer **5**, 510 (1981).

[9]J. Geiger, Z. Phys. A **282**, 129 (1977).

[10]R. B. King, J. Quant. Spectrosc. Radiat. Transfer **3**, 299 (1963).

[11]H. Puell and C. R. Vidal, Opt. Commun. **19**, 279 (1976).

[12]J. J. Wynne and R. Beigang, Phys. Rev. A **23**, 2736 (1981).

[13]R. Mahon and F. S. Thompkins, IEEE J. Quantum Electron. **QE-18**, 913 (1982).

[14]A. V. Smith and W. J. Alford, Phys. Rev. A **33**, 3172 (1986).
[15]D. Kramer, H. Chen, and M. G. Payne, Opt. Lett. **9**, 347 (1984).
[16]Y. M. Yiu, T. L. McIlrath, and R. Mahon, Phys. Rev. A **20**, 2470 (1979).
[17]M. G. Payne and W. R. Garrett, Phys. Rev. A **26**, 356 (1982).
[18]M. G. Payne and W. R. Garrett, Phys. Rev. A **28**, 3409 (1983).
[19]M. G. Payne, W. R. Garrett, and W. R. Ferrell, in *Resonance Ionization Spectroscopy*, edited by G. S. Hurst and M. G. Payne (Institute of Physics, Bristol, 1984), pp. 195—204.
[20]M. G. Payne, W. R. Garrett, and W. R. Ferrell, Phys. Rev. A **34**, 1143 (1986).
[21]J. C. Miller, R. N. Compton, M. G. Payne, and W. R. Garrett, Phys. Rev. Lett. **45**, 114 (1980).
[22]M. G. Payne, W. R. Ferrell, and W. R. Garrett, Phys. Rev. A **27**, 3053 (1983).
[23]W. R. Garrett, W. R. Ferrell, M. G. Payne, and J. C. Miller, Phys. Rev. A **34**, 1165 (1986).
[24]M. C. Castex, J. Chem. Phys. **66**, 3854 (1977).
[25]R. Wallenstein and H. Zacharias, Opt. Commun. **32**, 429 (1980).
[26]G. C. Bjorklund, IEEE J. Quantum Electron. **QE-11**, 287 (1975).
[27]A. Delage and J. D. Carette, Phys. Rev. A **14**, 1345 (1976).
[28]J. Koch, Fysiogr. Saellsk. Lund. Foerh. **19**, 2421 (1949).
[29]R. Mahon, T. J. McIlrath, and D. W. Koopman, Appl. Phys. Lett. **33**, 305 (1978).
[30]S. D. Kramer, M. G. Payne, and C. H. Chen, J. Opt. Soc. B **2**, 1284 (1985).
[31]P. J. Leonard, At. Data Nucl. Data Tables **14**, 22 (1974).
[32]R. Mahon, T. J. McIlrath, V. P. Myerscough, and D. W. Koopman, IEEE J. Quantum Electron. **QE-15**, 444 (1979).
[33]P. D. Chopra and D. W. O. Heddle, J. Phys. B **7**, 2421 (1974).